Universal Journal of Engineering Mechanics **1 (2013), 50 -70**
www.papersciences.com

A New Meshless Method for 2D Heat Transfer in Skin Tissues with Moving Boundary

Q. H. Qin and W. C. Zhang
Research School of Engineering, Australian National University, Canberra, ACT 2601, Australia
qinghua.qin@anu.edu.au

Abstract
A new meshless method is developed to investigate the behavior of heat conduction in isotropic biological tissues. The well-known Pennes' model associated with bio-heat equation is used for describing the process of heat conduction in skin tissues. To make the solution procedure simpler, the analog equation method is utilized to reconstruct the original bio-heat equation into an equivalent differential equation. Subsequently, the particular solution is approximated by the radial basis functions while the homogenous solution is approximately determined by the method of fundamental solution. The uniform structure of matrix is constructed by making use of the complete solution consisting of the particular and homogeneous parts satisfying the governing equation and the specified boundary conditions. The resulting equations are solved by a modified time stepping θ-method. Two examples of tumor hyperthermia and cryosurgery are considered to assess the accuracy and efficiency of the proposed method. It appears a promising method for detecting and evaluating the thermal damage of skin materials.

Key Word and Phrases
Bioheat Transfer, Radial Basis Function, Methods of Fundamental Solution.

Nomenclature

c	specific heat of tissue (J/kg/ ºC)	Q_r	spatial heating source (W/m^3)
c_b	specific heat of blood (J/kg/ ºC)	t	time (s)
h_∞	conventional coefficient (W/m^2/ ºC)	u	tissue temperature (ºC)
k	thermal conductivity of tissue (W/m/ ºC)	u_0	initial temperature (ºC)
k_f	thermal conductivity of frozen tissue (W/m/ ºC)	u_a	artery temperature (ºC)
k_u	thermal conductivity of unfrozen tissue (W/m/ ºC)	u_c	core temperature of tissue (ºC)
l	thickness (m)	u_e	environmental temperature (ºC)
L	depth of tissue (m)	u_{ml}	lower phase transition temperature (ºC)
q	normal heat flux (W/m^2)	u_{mu}	upper phase transition temperature (ºC)
Q_1	latent heat source (MJ/ m^3)	u_w	temperature contact with probe (ºC)
Q_m	metabolic heat source (W/m^3)	u_∞	environmental temperature (ºC)

1. Introduction

Studies on thermal behavior of biological tissues (for example, bone tissue [1,2], skin tissues[3-6]) has attracted significant attention during the past three decades. Generally, for biological tissue, the body surface temperature is controlled by the blood circulation underneath the skin, local metabolism, heat exchange between the skin and its environment, and the internal spatial heating like laser and microwave heating. Changes of any of these factors can induce variations of temperature at skin surface, reflecting the physiological state of the human body. Research on predictions of living tissue temperature is therefore important in many diagnostic applications.

Furthermore, the prediction of temperature distribution over the skin surface requires solutions to transient bioheat transfer problems. As a consequence, various numerical methods for simulating tissue temperature were developed during the past decades. So far, based on the most popular bioheat model, that is, the Pennes equation [7], the finite element method (FEM) [8-11], the finite difference method (FDM) [12,13], the Monte Carlo method (MCM) [14], and the boundary element method (BEM)/the dual reciprocity boundary element method (DRBEM) [15,16] have been well established to determine steady-state or transient temperature distribution in skin tissue. Among them, the FEM involving time-consuming domain discritization with finite cells is widely employed due to its good adaptability to complex shapes; the FDM depending on finite point difference net cannot osculate the coordinates of the complex biological shape; the BEM is an advantageous boundary-type method, which only involves the boundary discretization. However, it is difficult to treat transient or nonhomogeneous problems, in which the fundamental solutions used in conventional BEM [17] is required and domain integrals are usually hard to evaluate and time consuming. Fortunately, the appearance of DRBEM [15] based on the conventional BEM and radial basis functions can partly overcome these shortcomings. The remaining MCM is another special numerical method by way of random process, so it is different from the classic numerical methods listed above and depends weakly on the dimensions of the problem. Usually the MCM is viewed as a branch of experimental mathematics.

Unlike the above approaches, by the current research, a new meshless method based on combining the method of fundamental solutions, analog equation method, and radial basis functions (RBF) [18-21] is developed to predict the temperature distribution in skin tissues.

2. Problem statement and numerical procedure

2.1 Assumption

The skin of human being can usually be divided into three parts: epidermis, dermis and subcutaneous fat. They have different physical and chemical properties so that the skin can be viewed as composite materials which are not homogenous or isotropic. However, if only one single region such as epidermis or dermis is chosen for numerical computation, the skin can be considered as a homogenous and isotropic material. For simplicity, we assume that the skin is only composed of one single region which has the same physical and chemical properties. Therefore, the model can mathematically be set up based on the isotropic region of the skin. The analysis assumes that no interfacial resistance exists between the heating source and the skin surface.

2.2 Fundamentals of bioheat transfer

The bio-heat transfer equation developed by Pennes is here used to model the thermal behavior in skin tissue [3,7]:

$$\rho c \frac{\partial u}{\partial t} = \nabla (k \nabla u) + \omega_b \rho_b c_b (u_a - u) + Q_m + Q_r \tag{1}$$

where ρ is the density [kg/m^3] of the tissue, ρ_b is the density [kg/m^3] of blood, and ω_b is the blood perfusion rate [ml/s/ml].

From the Pennes' equation (1), it can be seen that the first expression on the right side describes the conduction of heat in the tissue which is induced by the temperature gradient. The second term stands for the heat flow transmission between the tissue and microcirculatory blood perfusion. The third term on the right hand side represents the internal heat generation due to metabolism and the last one is the spatial heating which is also called special heating. The internal tissues of the human beings have the ability to remove heat by both passive conduction and blood perfusion, which the Pennes' equation depicts. "The perfusion is defined as the non-vectorial volumetric blood flow per tissue volume in a region that contains sufficient capillaries that an average flow description is considered reasonable. Most tissues, including much of the skin and brain, are highly perfused, with a perfusion coefficient denoted by ω_b." [22].

Due to the single isotropic region of the skin tissue being analyzed, the thermal conductivity *k* is

constant during the whole process. In this case, the Pennes' bio-heat equation can then be rewritten as:

$$\rho c \frac{\partial u(\mathbf{x},t)}{\partial t} = k\nabla^2 u(\mathbf{x},t) + \omega_b \rho_b c_b \left(u_a - u(\mathbf{x},t)\right) + Q_m + Q_r \tag{2}$$

where the transient heat conduction problem occupies an arbitrarily shaped region Ω bounded by its boundary Γ (see Figure 1), the bold letter **x** indicates the two-dimensional Cartesian coordinate vector, and Q_m, Q_r are assumed to be the function of x, y, t. Temperature-dependent perfusion coefficient ω_b and moving boundary (see Section 3.2) are two possible non-linear aspects of Pennes model. Besides the above bioheat governing equation, the corresponding boundary conditions and initial condition should be provided to make the system solvable:

1) Dirichlet boundary condition related to unknown temperature field is

$$u(\mathbf{x},t) = \overline{u}(\mathbf{x},t) \qquad \mathbf{x} \in \Gamma_1 \tag{3}$$

2) Neumann boundary condition for the boundary heat flux is

$$q_n(\mathbf{x},t) = \overline{q}_n(\mathbf{x},t) \qquad \mathbf{x} \in \Gamma_2 \tag{4}$$

3) Convection or Robin boundary condition is

$$q_n(\mathbf{x},t) = h_\infty (u - u_\infty) \quad \text{or} \quad h_\infty u - q_n = h_\infty u_\infty \quad \mathbf{x} \in \Gamma_3 \tag{5}$$

or in a general form

$$\beta_1 u(\mathbf{x},t) + \beta_2 q(\mathbf{x},t) = \beta_0(\mathbf{x},t) \qquad \mathbf{x} \in \Gamma \tag{6}$$

4) Initial condition is

$$u\left(\mathbf{x},0\right) = u_0 \qquad \mathbf{x} \in \Omega \tag{7}$$

where $q_n = -k\dfrac{\partial u}{\partial n_i}$ and n_i are the components of the unit outward normal to the boundary Γ. $\overline{u}$ and $\overline{q}_n$ are specified values of temperature and heat flux on the boundary, β_0, β_1 and β_2 are known coefficients.

For a well-posed problem, we have $\Gamma = \Gamma_1 \cup \Gamma_2 \cup \Gamma_3$. It is noted that the convection boundary condition is in fact a type of Robin mixed boundary condition [21].

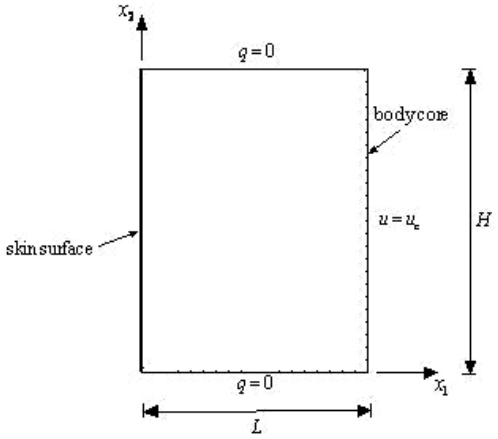

Fig. 1 Diagram of a typical single-layer tissue

2.3 Analog equation method (AEM)

The analog equation method (AEM) is used to convert the boundary value problems (BVPs) described by (2)-(5) into a Poisson-type equation. For this purpose, suppose $u(\mathbf{x})$ is the sought solution to the BVPs, which is a continuously differentiable function with up to two orders in domain Ω [21]. Therefore, (2) can be rewritten as follows:

$$\nabla^2 u(\mathbf{x},t) = \frac{\rho c}{k}\cdot\frac{\partial u(\mathbf{x},t)}{\partial t} - \frac{\omega_b \rho_b c_b}{k}\left(u_a - u(\mathbf{x},t)\right) - \frac{Q_m}{k} - \frac{Q_r}{k} \tag{8}$$

Denoting $b(\mathbf{x},t) = \frac{\rho c}{k}\cdot\frac{\partial u(\mathbf{x},t)}{\partial t} - \frac{\omega_b \rho_b c_b}{k}\left(u_a - u(\mathbf{x},t)\right) - \frac{Q_m}{k} - \frac{Q_r}{k}$, (8) becomes

$$\nabla^2 u(\mathbf{x},t) = b(\mathbf{x},t) \qquad \mathbf{x}\in\Omega \tag{9}$$

(9) shows that the solution of (2) cannot be determined by solving this linear equation with the boundary conditions (3) - (5) unless the fictitious source distribution $b(\mathbf{x},t)$ is known. Considering that (9) is an inhomogeneous linear differential equation, its solution can be divided into two parts: one is the general solution to homogeneous equation while another is the particular solution to the inhomogeneous equation (9). So we can express the solution in terms of the general solution u_{hom} and particular solution u_{par} as

$$u = u_{\text{hom}} + u_{\text{par}} \tag{10}$$

Consequently, the solutions u_{hom} and u_{par} should satisfy following two equations:

$$\nabla^2 u_{\text{hom}}(\mathbf{x},t) = 0 \qquad \mathbf{x}\in\Omega \tag{11}$$

$$\nabla^2 u_{\text{par}}(\mathbf{x},t) = b(\mathbf{x},t) \qquad \mathbf{x}\in\Omega \tag{12}$$

The boundary conditions (3)-(5) should be modified as

$$\begin{cases} u_{\text{hom}}(\mathbf{x},t) = \overline{u}(\mathbf{x},t) - u_{\text{par}}(\mathbf{x},t) & \mathbf{x}\in\Gamma_1 \\ q_{\text{nhom}}(\mathbf{x},t) = \overline{q}_n(\mathbf{x},t) - q_{\text{npar}}(\mathbf{x},t) & \mathbf{x}\in\Gamma_2 \\ h_\infty u_{\text{hom}}(\mathbf{x},t) - q_{\text{nhom}}(\mathbf{x},t) = h_\infty u_\infty - h_\infty u_{\text{par}}(\mathbf{x},t) + q_{\text{npar}}(\mathbf{x},t) & \mathbf{x}\in\Gamma_3 \end{cases} \tag{13}$$

2.4 Radial basis functions (RBFs)

RBFs are used to evaluate the particular solution approximately. According to Ref. [23], RBFs are generally viewed as "such functions that depend only on the Euclidean distance between any field point and a reference point (sometimes the central point of the element under consideration), so they are completely isotropic and can be easily used for scattered data interpolation in multi-dimensional space". For this purpose, the right-hand side of (12) can be approximated by a sum of linear RBFs as

$$b(\mathbf{x},t)=\sum_{j=1}^{I+B}\alpha_j(t)b_j(\mathbf{x}) \qquad \mathbf{x}\in\Omega \tag{14}$$

where I and B are the number of interpolation points in the domain and on the boundary respectively as shown in Figure 2. α_j is a series of special coefficients to be evaluated. Furthermore, let $b_j(\mathbf{x})=b(r_j)$ where r_j represents the Euclidean distance from the central point $\mathbf{x}_j$ inside the domain to an arbitrary point **x** in the domain or on the :

$$r_j=\left|\mathbf{x}-\mathbf{y}_j\right|=\sqrt{(x_1-y_{1j})^2+(x_2-y_{2j})^2}\ .$$

Correspondingly, the particular solution can be approximated as

$$u_{\text{par}}(\mathbf{x},t)=\sum_{j=1}^{I+B}\alpha_j(t)\hat{u}_j(\mathbf{x}) \qquad \mathbf{x}\in\Omega \tag{15}$$

where $\hat{u}_j(\mathbf{x})$ corresponds to a set of particular solutions which have a close relationship with $b_j(\mathbf{x})$ [see (18)].

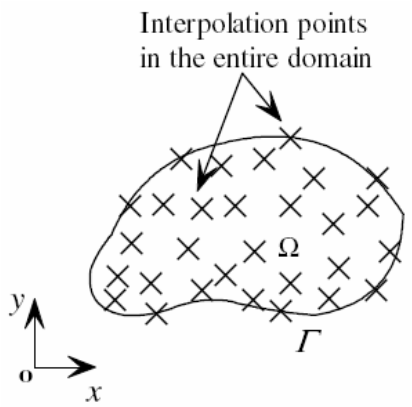

Fig. 2 Schematic of interpolation points in the domain and on the boundary

Substituting (14) and (15) into (12), we obtain

$$\nabla^2\left(\sum_{j=1}^{I+B}\alpha_j(t)\hat{u}_j(\mathbf{x})\right)=\sum_{j=1}^{I+B}\alpha_j(t)b_j(\mathbf{x}) \qquad \mathbf{x}\in\Omega \tag{16}$$

If the unknown coefficient α_j is not zero α_j we have from (16) that

$$\nabla^2\left(\sum_{j=1}^{I+B}\hat{u}_j(\mathbf{x})\right)=\sum_{j=1}^{I+B}b_j(\mathbf{x}) \qquad \mathbf{x}\in\Omega \tag{17}$$

as α_j is an independent constant. (12) can then be simply written as

$$\nabla^2 \hat{u}_j = b_j \tag{18}$$

Using the expression of heat flux $q_n = -k\dfrac{\partial u}{\partial n_i}$, the particular heat flux over the boundary can be written in the form

$$q_{\text{npar}}(\mathbf{x},t) = -k\frac{\partial u_{\text{par}}(\mathbf{x},t)}{\partial n_i} = -k\sum_{j=1}^{I+B}\alpha_j(t)\cdot\frac{\partial \hat{u}_j(\mathbf{x})}{\partial n_i} \tag{19}$$

As indicated in [23], there are two types of RBFs used in numerical computations. One is the piecewise polynomial compactly supported RBF (CS-RBF) while the other is the globally supported RBF (GS-RBF). The difference between these two methods is the domain under consideration. For CS-RBF, the user can select the support domain which satisfies the positive definite for a given order smoothness. However, GS-RBF is concerned as the whole domain under consideration. Table 1 lists some common used RBFs.

Table 1 Some common used RBFs [23]

Categories	Name	RBF expression
Piecewise smooth RBFs	Power spline (PS)	$\phi_j(\mathbf{x}) = r_j^{2n-1}$
	Thin plate spline (TPS)	$\phi_j(\mathbf{x}) = r_j^{2n}\ln r_j$
Infinitely smooth RBFs	Multi-quadric (MQ)	$\phi_j(\mathbf{x}) = \sqrt{r_j^2 + c^2}$
	Gaussian (GS)	$\phi_j(\mathbf{x}) = e^{-r_j^2}$

In this study, PS is primarily used for our examples discussed later. Thus, making use of $b_j(\mathbf{x}) = r_j^{2n-1}$ (18) becomes

$$\nabla^2 \hat{u}_j = r_j^{2n-1} \tag{20}$$

Considering $r_j = \left|\mathbf{x}-\mathbf{y}_j\right| = \sqrt{(x_1-y_{1j})^2+(x_2-y_{2j})^2}$, the Laplacian operator ∇^2 can be expressed in terms of polar coordinate r as follows:

$$\begin{aligned}
&\frac{1}{r}\frac{\partial}{\partial r}\left(r\frac{\partial \hat{u}}{\partial r}\right) = r^{2n-1} \qquad \Rightarrow \frac{\partial}{\partial r}\left(r\frac{\partial \hat{u}}{\partial r}\right) = r^{2n} \\
&r\frac{\partial \hat{u}}{\partial r} = \int r^{2n} = \frac{r^{2n+1}}{2n+1} \qquad \Rightarrow \frac{\partial \hat{u}}{\partial r} = \frac{r^{2n}}{2n+1} \\
&\hat{u} = \int \frac{r^{2n}}{2n+1} = \frac{r^{2n+1}}{(2n+1)^2}
\end{aligned} \tag{21}$$

In particular, if the order *n* is equal to 1, $b_j(\mathbf{x}) = r_j$ and the corresponding function $\hat{u}$ has the form $\hat{u}_j = r_j^3/9$. However, from (14), it is obvious that the unknown coefficients $\alpha_j(t)$ cannot be straightly determined since the inhomogeneous term $b_j(\mathbf{x})$ depends on the unknown temperature field $u_j(\mathbf{x})$. A virtual point collocation method is developed to determine the coefficient $\alpha_j(t)$ in the next two sub-sections.

2.5 Virtual boundary point collocation method (VBCM)

If N fictitious nodal points $Y_i(i=1,2,\cdots,N)$ on the virtual boundary are selected corresponding to N real nodal points $X_i(i=1,2,\cdots,N)$ on the physical boundary, a virtual source load $\varphi_i(i=1,2,\cdots,N)$ is applied to each fictitious source point. Similarly to the basic idea of MFS, the homogeneous temperature field u_{hom} can be expressed by a linear combination of fundamental solutions compared to the fictitious sources located on the virtual boundary.

$$u_{\text{hom}}(\mathbf{x},t)=\sum_{i=1}^{N}\varphi_i(t)u_i^*(\mathbf{x}) \qquad \mathbf{x}\in\Omega \tag{22}$$

where φ_i is a set of unknown coefficients to be determined, $u_i^*(\mathbf{x})=u^*(\mathbf{x}_i,\mathbf{y}_i)$ are the fundamental solutions of the Laplacian operator and $\mathbf{y}_i$ is the set of fictitious source points outside the physical boundary under consideration (see Figure 3). Additionally, the heat flux normal to the boundary can be expressed as

$$q_{\text{nhom}}(\mathbf{x},t)=-k\cdot\frac{\partial u_{\text{hom}}(\mathbf{x},t)}{\partial n_i}=-k\cdot\sum_{i=1}^{N}\varphi_i(t)\cdot\frac{\partial u^*(\mathbf{x}_i,\mathbf{y}_i)}{\partial n_i} \tag{23}$$

It is obvious that (22) satisfy the homogenous equation (11) in nature due to the definition of the fundamental solutions.

$$\nabla^2 u^*(\mathbf{x}_i,\mathbf{y}_i)=\delta(\mathbf{x}_i,\mathbf{y}_i) \qquad \forall\mathbf{x},\mathbf{y}_i\in R^2 \tag{24}$$

where δ is a standard Delta function satisfying

$$\delta\left(\mathbf{x},\mathbf{x}_i'\right)=\begin{cases}0 & \mathbf{x}\neq\mathbf{y}_i\\ \infty & \mathbf{x}=\mathbf{y}_i\end{cases} \tag{25}$$

The typical solution to (24) in two-dimensional cases is written as [21]:

$$u^*(\mathbf{x}_i,\mathbf{y}_i)=\frac{1}{2\pi}\ln\frac{1}{r(\mathbf{x}_i,\mathbf{y}_i)} \tag{26}$$

where $r(\mathbf{x}_i,\mathbf{y}_i)$ represents the Euclidean distance from the field points $\mathbf{x}_i$ to the fictitious source points $\mathbf{y}_i$ on the virtual boundary: $r(\mathbf{x}_i,\mathbf{y}_i)=\left|\mathbf{x}_i-\mathbf{y}_i\right|=\sqrt{(x_{1i}-y_{1i})^2+(x_{2i}-y_{2i})^2}$.

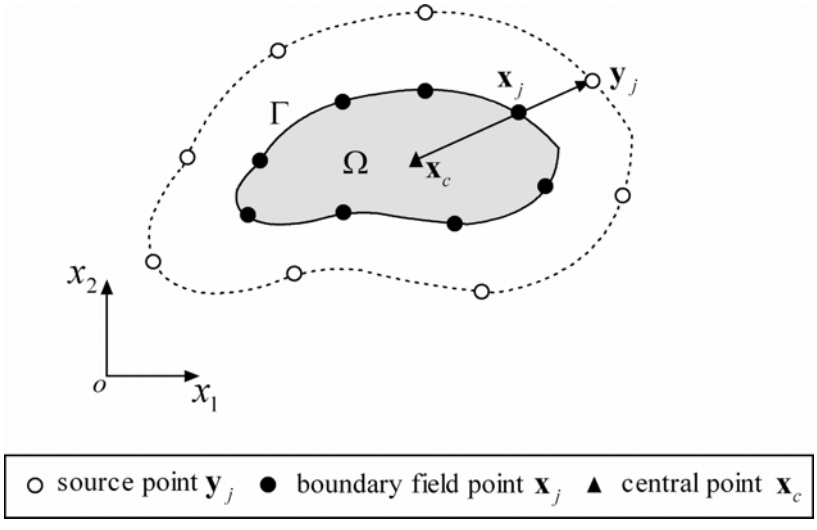

Fig. 3 Schematic of source points and boundary field points

In addition, the problem for the generation of source points outside the domain, which contributes to the accuracy and stability of numerical computing system, attracts a wide range of interests. However, no standardized technique can be used to generate these source points effectively and properly. In this case, linear interpolation method is used as shown in Figure 3:

$$\mathbf{y}_i = \mathbf{x}_i + \gamma(\mathbf{x}_i - \mathbf{x}_c) \tag{27}$$

where $\mathbf{x}_c$ is the central point of the domain (see Figure 3). The interpolating coefficient γ is a dimensionless parameter. Determination of the optimal value of γ was discussed in [24]. Further, it should be mentioned that the number of fictitious source points on the virtual boundary is identical to that of nodes on the real boundary in the proposed meshless method due to the convenience of computing. Actually, the reasonable number of these points exists, which can have a significantly critical impact on the minimal possible computing time and represent all the boundary conditions [21].

2.6 Construction of linear equations for determining α_j and φ_i

An equation system for determining the desired temperature field $u(\mathbf{x},t)$ can be obtained by substituting (15) and (22) into (10) as

$$u(\mathbf{x},t) = u_{\text{par}} + u_{\text{hom}} = \sum_{j=1}^{I+B} \alpha_j(t)\hat{u}_j(\mathbf{x}) + \sum_{i=1}^{N} \varphi_i(t) u_i^*(\mathbf{x}) \qquad \mathbf{x} \in \Omega \tag{28}$$

The solution of (28) is the approximate numerical solution for the original problem defined by (2) with the conditions (3)-(5).

It is convenient for computer programming with Matlab or C to utilize the matrix form. Therefore, (28) is rewritten in the matrix form as

$$u(\mathbf{x},t) = \{U(\mathbf{x})\}\{A(t)\} \qquad \mathbf{x} \in \Omega \tag{29}$$

where

$$\{U(\mathbf{x})\} = \left\{\hat{u}_1(\mathbf{x}), \quad \hat{u}_2(\mathbf{x}) \quad \cdots \quad \hat{u}_M(\mathbf{x}), \quad u_1^*(\mathbf{x}), \quad u_2^*(\mathbf{x}) \quad \cdots \quad u_N^*(\mathbf{x})\right\}_{M+N} \quad \mathbf{x} \in \Omega$$

$$\{A(t)\} = \{\alpha_1(t), \quad \alpha_2(t) \quad \cdots \quad \alpha_M(t), \quad \varphi_1(t), \quad \varphi_2(t) \quad \cdots \quad \varphi_N(t)\}_{M+N}^T$$

and $M = I + B$.

Accordingly, the heat flux normal to the boundary can be expressed as:

$$q_n(\mathbf{x},t) = \{Q(\mathbf{x})\}\{A(t)\} \qquad \mathbf{x} \in \Omega \tag{30}$$

where

$$\{Q(\mathbf{x})\} = -k\left\{\frac{\partial \hat{u}_1(\mathbf{x})}{\partial n_i}, \quad \frac{\partial \hat{u}_2(\mathbf{x})}{\partial n_i} \quad \cdots \quad \frac{\partial \hat{u}_M(\mathbf{x})}{\partial n_i}, \quad \frac{\partial u_1^*(\mathbf{x})}{\partial n_i}, \quad \frac{\partial u_2^*(\mathbf{x})}{\partial n_i} \quad \cdots \quad \frac{\partial u_N^*(\mathbf{x})}{\partial n_i}\right\}_{M+N} \quad \mathbf{x} \in \Omega$$

Furthermore, by using the vector convention, the boundary conditions (3)-(5) and (7) are rewritten as

$$\begin{cases} \{U(\mathbf{x})\}\{A(t)\} = \overline{u}(\mathbf{x},t) & \mathbf{x}\in\Gamma_1 \\ \{Q(\mathbf{x})\}\{A(t)\} = \overline{q}(\mathbf{x},t) & \mathbf{x}\in\Gamma_2 \\ \{Q(\mathbf{x})\}\{A(t)\} = h_\infty \{U(\mathbf{x})\}\{A(t)\} - h_\infty u_\infty & \mathbf{x}\in\Gamma_3 \end{cases} \tag{31}$$

or a general form

$$\beta_1 \{U(\mathbf{x})\}\{A(t)\} + \beta_2 \{Q(\mathbf{x})\}\{A(t)\} = \beta_0(\mathbf{x},t) \qquad \mathbf{x}\in\Gamma \tag{32}$$

and the initial condition is

$$\{U(\mathbf{x})\}\{A(t)\}\big|_{t=0} = u_0 \qquad \mathbf{x}\in\Omega \tag{33}$$

(2) can be also rewritten as

$$\rho c \cdot \{U(\mathbf{x}_j)\}\{\dot{A}(t)\} = k\cdot\nabla^2\{U(\mathbf{x}_j)\}\cdot\{A(t)\} + \omega_b\rho_b c_b\left(u_a - \{U(\mathbf{x}_j)\}\{A(t)\}\right) + Q_m + Q_r \qquad (j=1,2\cdots M) \tag{34}$$

(34) can be re-arranged in the form

$$\rho c\{U(\mathbf{x}_j)\}\cdot\{\dot{A}(t)\} + \left(\omega_b\rho_b c_b\{U(\mathbf{x}_j)\} - k\nabla^2\{U(\mathbf{x}_j)\}\right)\cdot\{A(t)\} = \omega_b\rho_b c_b u_a + Q_m + Q_r \qquad (j=1,2\cdots M) \tag{35}$$

with the boundary condition (32) in terms of $A(t)$ as

$$\{0\}\cdot\{\dot{A}(t)\} + \left(\beta_1\{U(\mathbf{x}_i')\} + \beta_2\{Q(\mathbf{x}_i')\}\right)\cdot\{A(t)\} = \beta_0(\mathbf{x}_i',t) \qquad (i=1,2\cdots N) \tag{36}$$

In order to determine all unknowns, let (35) to be satisfied at M points $\mathbf{x}_j$ in the domain and the boundary conditions (36) to be satisfied at N boundary field points $\mathbf{x}_i$ so that a linear equation system can be constructed as:

$$[M]\{\dot{A}\} + [K]\{A\} = \{F\} \tag{37}$$

where

$$[M] = \rho c \begin{bmatrix} \{U(\mathbf{x}_1)\} \\ \{U(\mathbf{x}_2)\} \\ \vdots \\ \{U(\mathbf{x}_M)\} \\ 0 \\ 0 \\ \vdots \\ 0 \end{bmatrix}_{(M+N)\times(M+N)} \qquad [K] = \begin{bmatrix} \omega_b\rho_b c_b\{U(\mathbf{x}_1)\} - k\nabla^2\{U(\mathbf{x}_1)\} \\ \omega_b\rho_b c_b\{U(\mathbf{x}_2)\} - k\nabla^2\{U(\mathbf{x}_2)\} \\ \vdots \\ \omega_b\rho_b c_b\{U(\mathbf{x}_M)\} - k\nabla^2\{U(\mathbf{x}_M)\} \\ \beta_1\{U(\mathbf{x}_1')\} + \beta_2\{Q(\mathbf{x}_1')\} \\ \beta_1\{U(\mathbf{x}_2')\} + \beta_2\{Q(\mathbf{x}_2')\} \\ \vdots \\ \beta_1\{U(\mathbf{x}_N')\} + \beta_2\{Q(\mathbf{x}_N')\} \end{bmatrix}_{(M+N)\times(M+N)}$$

$$\{A(t)\} = \{\alpha_1(t),\quad \alpha_2(t)\quad\cdots\quad \alpha_M(t),\quad \varphi_1(t),\quad \varphi_2(t)\quad\cdots\quad \varphi_N(t)\}^T_{M+N}$$

$$\{\dot{A}(t)\} = \left\{\frac{d\alpha_1(t)}{dt},\quad \frac{d\alpha_2(t)}{dt}\quad\cdots\quad \frac{d\alpha_M(t)}{dt},\quad \frac{d\varphi_1(t)}{dt},\quad \frac{d\varphi_2(t)}{dt}\quad\cdots\quad \frac{d\varphi_N(t)}{dt}\right\}^T_{M+N}$$

and

$$\{F\}=\begin{bmatrix} f(\mathbf{x}_1,t) \\ f(\mathbf{x}_2,t) \\ \vdots \\ f(\mathbf{x}_M,t) \\ \beta_0(\mathbf{x}'_1,t) \\ \beta_0(\mathbf{x}'_2,t) \\ \vdots \\ \beta_0(\mathbf{x}'_M,t) \end{bmatrix}_{M+N}$$

with $f(\mathbf{x}_j,t)=\omega_b\rho_b c_b u_a+Q_m(\mathbf{x}_j,t)+Q_r(\mathbf{x}_j,t) \quad (j=1,2\cdots M)$

(37) can be used for problems without moving boundary. The treatment of moving boundary is described in Section 3.2.

2.7 Time stepping θ-method

From (37), it is apparent that both coefficient vectors $[M]$ and $[K]$ are independent of time t, Additionally, $\{F\}$ is composed of known functions of the time t and the position vector **x** which can be determined without using any information of unknowns. Therefore, (37) is a first order time derivative problem which can be solved using time stepping θ-method [25]. With the time stepping θ-method, the time domain is divided into a number of small intervals $[t_n, t_{n+1}]$ $(n=0,1,2\cdots)$ and the time step is denoted as the difference between the beginning and the end of the interval: $\Delta t=t_{n+1}-t_n$. If a typical time interval $[t_0, t_1]$ is considered, (37) can be written at these two consecutive time steps "0" and "1" as follows:

$$\begin{cases} [M]\{\dot{A}\}_0+[K]\{A\}_0=\{F\}_0 \\ [M]\{\dot{A}\}_1+[K]\{A\}_1=\{F\}_1 \end{cases} \tag{38}$$

Furthermore, to obtain the solution from the status "0" to "1", a weighted average of the gradients at the beginning and end of the time interval is utilized [25]. Thus,

$$\{A\}_1=\{A\}_0+\Delta t\left((1-\theta)\{\dot{A}\}_0+\theta\{\dot{A}\}_1\right) \tag{39}$$

From (38), we obtain

$$\begin{cases} \{\dot{A}\}_0=-\dfrac{[K]}{[M]}\{A\}_0+\dfrac{\{F\}_0}{[M]} \\ \{\dot{A}\}_1=-\dfrac{[K]}{[M]}\{A\}_1+\dfrac{\{F\}_1}{[M]} \end{cases} \tag{40}$$

Then, Substituting (40) into (39) to eliminate the time derivative yields

$$\{A\}_1 = \{A\}_0 + \Delta t\left((1-\theta)\left(-\frac{[K]}{[M]}\{A\}_0 + \frac{\{F\}_0}{[M]}\right) + \theta\left(-\frac{[K]}{[M]}\{A\}_1 + \frac{\{F\}_1}{[M]}\right)\right)$$

$$\Rightarrow \left([M]+\theta[K]\Delta t\right)\{A\}_1 = \left([M]-(1-\theta)[K]\Delta t\right)\{A\}_0 + (1-\theta)\Delta t\{F\}_0 + \theta\Delta t\{F\}_1 \quad (41)$$

$$\Rightarrow \left(\frac{[M]}{\Delta t}+\theta[K]\right)\{A\}_1 = \left(\frac{[M]}{\Delta t}-(1-\theta)[K]\right)\{A\}_0 + (1-\theta)\{F\}_0 + \theta\{F\}_1$$

As in Ref. [25], it is noted that the system is unconditionally 'stable' (i.e. errors will not grow unboundedly) only if $\theta \geq 1/2$. In addition, considering two extremes of θ, if the moment $\{F\}$ is assumed to be zero, when $\theta = 1/2$, it leads to the Crank-Nicolson method, thus,

$$\left([M]+\frac{\Delta t}{2}[K]\right)\{A\}_1 = \left([M]-\frac{\Delta t}{2}[K]\right)\{A\}_0 \quad (42)$$

and when $\theta = 1$ giving the fully implicit method, thus,

$$\left([M]+[K]\Delta t\right)\{A\}_1 = [M]\{A\}_0 \quad (43)$$

3. Numerical Assessment

Here we consider two cases of transient heat transfer in skin tissues, including tissue with tumor and cryosurgery. It should be mentioned here that the purpose of these two examples is to provide an insight into the performance and the applicability of the proposed numerical method.

3.1 Tumor hyperthermia

If there is a tumor at the skin surface, the tumor will affect the distribution of blood perfusion due to different metabolic heat generation. The different thermal state expressions at the skin surface will indicate the abnormal blood perfusion or metabolic heat generation. It is a benefit that this difference can be used for noninvasive diagnostics for the physiological status of the biological body such as tumor [26].

To demonstrate this as well as the efficiency of the proposed method, a classical example is considered. Figure 4 shows the boundary definition and the domain used in this example. In the analysis, 56 boundary nodes on the real boundary and 231 interpolation nodes within the domain are employed.

The boundary conditions used are shown as below:

$$q(x,y;0) = 0, \qquad x,y \in \textit{I}\ ,\textit{II}\ ,\textit{IV}$$

$$T(x,y;0) = 37^{\circ}\mathrm{C}, \qquad x,y \in \textit{III}$$

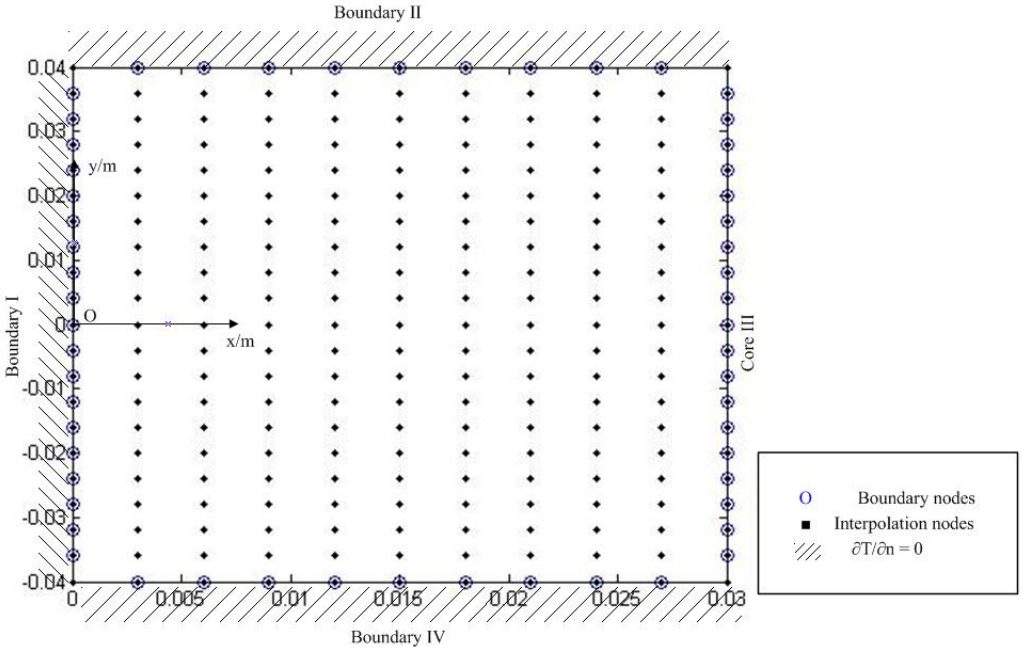

Fig. 4 Schematic of boundary definition and used domain

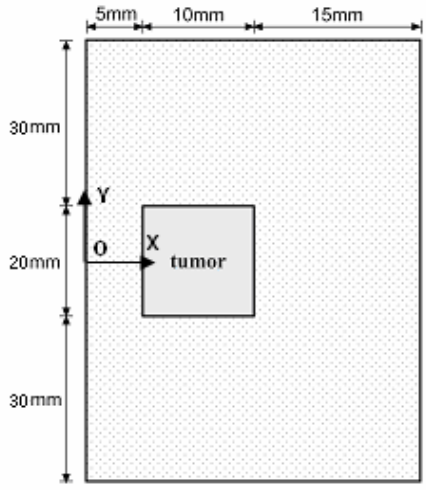

Fig. 5 Illustration of tissue with tumor

For simplicity, the environmental parameters are neglected in this example. In practice, an insulating material can be used to cover the skin boundary for preventing the influence from the surrounding environment. The insulating material is assumed to be large enough to permit the temperature inside the body to reach the steady state. The temperature at core III boundary is considered as constant as well as arterial blood temperature is assumed to be u_a=37°C [26,27]. As indicated by Dudar and Jain [28], the malignant tumor often causes significantly diverse blood perfusion rates at the tumor site and the surrounding tissues. However, since there is a lack of experimental measurements for these parameters, the parameters given in Refs. [26,27] are adopted. Essentially, we assume that $\omega_b = 0.0005\text{ml/s/ml}, x, y \in \Omega$, $Q_m = 420\text{J/m}^3\text{s}, x, y \in \Omega$ for healthy tissue, while

$$\omega_b = \begin{cases} 0.0005\text{ml/s/ml}, x, y \notin L \\ 0.002\text{ml/s/ml}, x, y \in L \end{cases}, \quad Q_m = \begin{cases} 420\text{J/m}^3\text{s}, x, y \notin L \\ 4200\text{J/m}^3\text{s}, x, y \in L \end{cases}$$

for tissue with a tumor, where $L \subseteq \left[|y| \le 0.01m,\ 0.005m \le x \le 0.015m \right]$ is prearranged as tumor domain and Ω is the solution domain shown in Figure 5. The density of tissue ρ is $1.0 \times 10^3\,\text{kg/m}^3$ and the thermal conductivity of the tissue k is 0.5 W/m·°C.

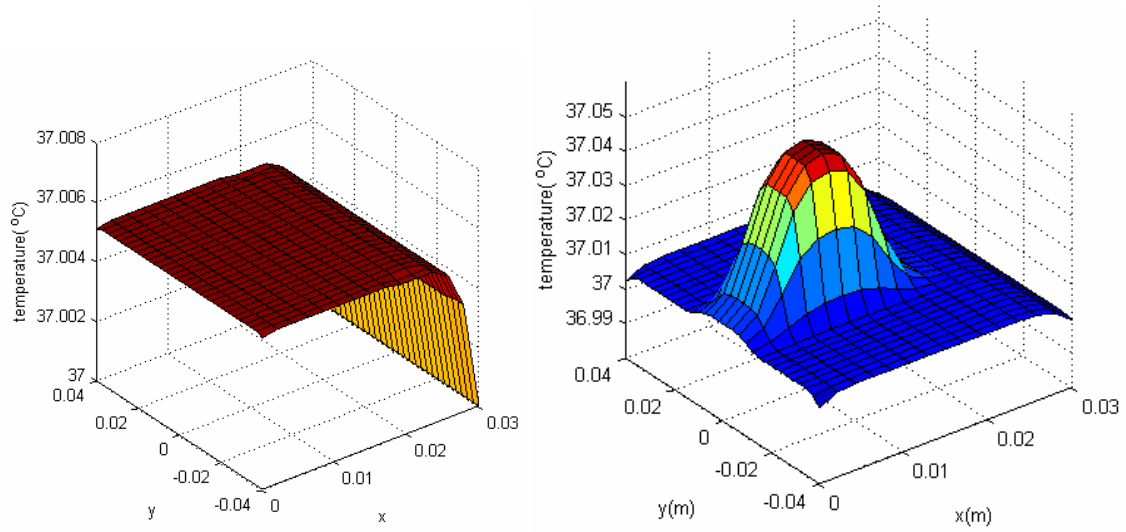

(a) t = 50s

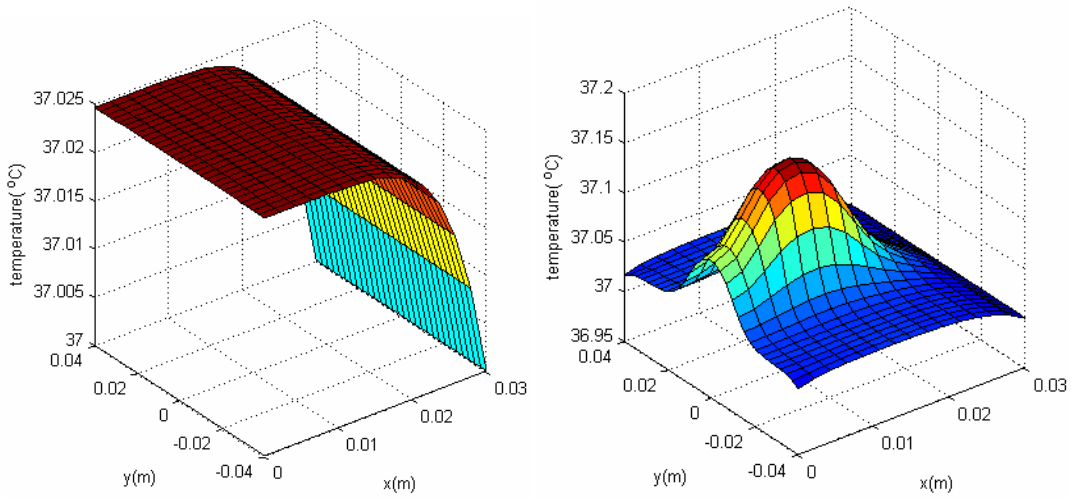

(b) t = 250s

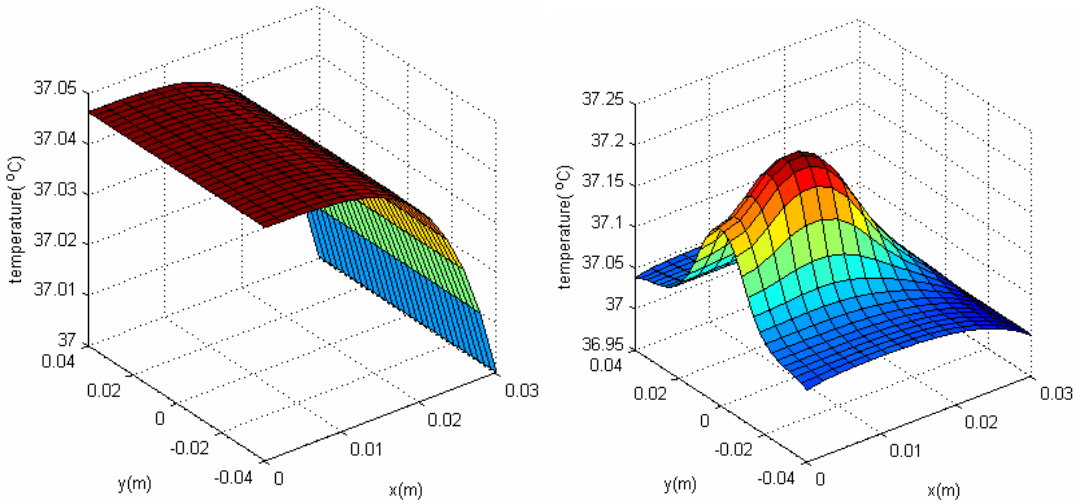

(c) t = 500s

Fig. 6 Dynamic temperature distributions in two tissues

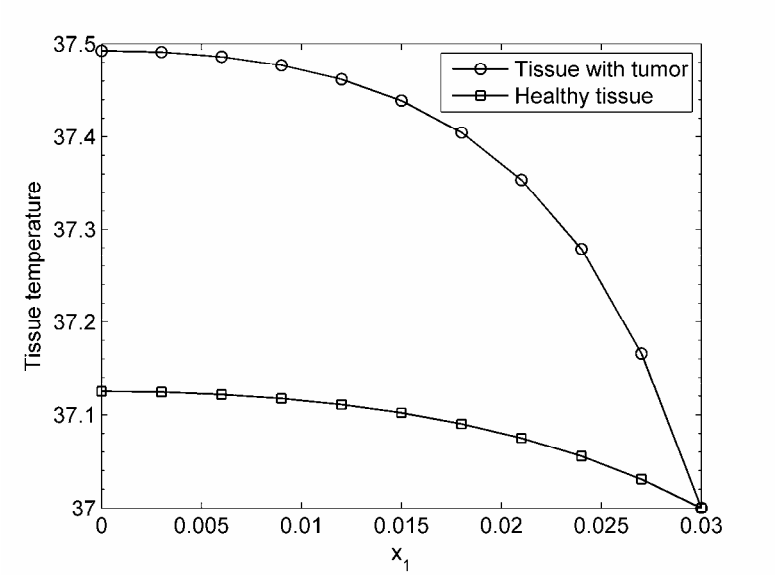

Fig. 7 Comparison of tissue temperature along the depth of skin for healthy and abnormal tissues

Figure 6 represents different temperature profiles at different time when theta is 0.6 and Δt is 10s. At the beginning, the numerical profiles for both cases are quite different. Additionally, when the time elapses, the temperature in tumor sites will increase dramatically due to a high blood perfusion and metabolic heat generation. After about 30 minutes and 38 minutes, the steady states for tissue with tumor and healthy tissue are achieved and the temperature along the depth of the skin tissue is plot in Figure 7, from which the distinct difference between two tissues is observed due to different blood perfusions and metabolic heats.

3.2 Cryosurgery

Cryosurgery is a freezing technique used in the clinic medical surgery for the cancer or tumors. It utilizes tremendously low temperature into frozen range in situ to kill or remove cancer tissues or tumors in target. Cryosurgery can select undesirable area to destroy. It has been used in various medical surgeries for different parts of bodies by a large number of surgeons, doctors and experts, especially when the targeted tissues can be easily accessed. The specialists in general implement the surgery by using one or several cryoprobes on account of the low temperature, actually below freezing point, utilized in cryosurgery, which will form ice crystals and destruct the cell membranes. The cryoprobe typically has a shape of nitrogen-perfuse hollow cylinder. The diameter of cryoprobes usually has a variety from 2 to 20mm. The tip of cryoprobe will induce the freezing temperature while other parts will insulate the tissues. Although the cryosurgery can be found in many areas, such as dermatology, gynecology, urology, orthopedics, otology, neurosurgery, ophthalmology, the cancer management etc, there are several main difficult problems arising from this technology. One of main problems is hard to understand the extent of the irregular shape of the freezing section. Others are the direction of ice growth and the temperature distribution within ice balls during the freezing process. Furthermore, the healthy tissues around the targeted tumors are unintended to be removed in some cases[14]. Therefore, it is necessary to understand the development of ice balls and temperature distribution during the preceding cryosurgery very well. The algorithm proposed in this paper can handle these problems with moving boundary. Problems associated with moving boundary is in fact highly non-linear due to the unknowns on the position of ice front, the direction and velocity of ice surface growth [14].

Making use of the Pennes bio-heat equation, the process of heat transfer in unfrozen region of the skin tissue is governed by:

$$\rho_u c_u \frac{\partial u_u(\mathbf{x},t)}{\partial t} = k_u \nabla^2 u_u(\mathbf{x},t) + \omega_b \rho_b c_b \left(u_a - u_u(\mathbf{x},t)\right) + Q_m \tag{44}$$

where ρ_u and c_u are density and specific heat in unfrozen tissue respectively. k_u is thermal conductivity of unfrozen tissue, $u_u(\mathbf{x},t)$ is temperature to be found in unfrozen tissue.
In frozen area, the bio-heat equation is reduced to

$$\rho_f c_f \frac{\partial u_f(\mathbf{x},t)}{\partial t} = k_f \nabla^2 u_f(\mathbf{x},t) \tag{45}$$

for the reason that blood perfusion and metabolic generation will cease due to low temperature, where ρ_f and c_f are the density and specific heat in the frozen tissues respectively, and $u_f(\mathbf{x},t)$ is the temperature in frozen tissue.

By assuming that the tissue is ideal enough so that the density of this biological tissue ρ is constant which means that the density in liquid phase is the same as that in solid phase. The conditions for the temperature continuity and energy balance at the moving interface are given by

$$u_u(\mathbf{x},t) = u_f(\mathbf{x},t) = u_m \qquad \mathbf{x} \in \Gamma_m \tag{46}$$

$$k_f \frac{\partial u_f(\mathbf{x},t)}{\partial n} - k_u \frac{\partial u_u(\mathbf{x},t)}{\partial n} = Q_1 v_n \qquad \mathbf{x} \in \Gamma_m \tag{47}$$

where u_m is frozen temperature in the targeted tissue, and n is the unit outward normal to the moving boundary Γ_m, and v_n is denoted as the normal velocity of moving interface.

Such problems are considered highly non-linear. Direct discretion of the governing equations will not converge to the approximated solution by iteration at the moving boundary. To prevent this iterative divergence. First, the effective heat capacity method is used to construct a uniform and linear equation [29]. Subsequently, the linear equation is solved using the proposed algorithm.

Before utilizing the effective heat capacity method, the uniform equation can be formed by means of (44) and (45) as:

$$\Lambda \frac{\partial u(\mathbf{x},t)}{\partial t} = k(u)\nabla^2 u(\mathbf{x},t) + \omega_b(u) C_b \left(u_a - u_u(\mathbf{x},t)\right) + Q_m(\mathrm{u}) \tag{48}$$

where $\Lambda = C(u) + Q_1 \delta(u - u_m)$, $\delta(u - u_m)$ is Dirac delta function, and:

$$k(u) = \begin{cases} k_f, & \mathrm{u<u_m} \\ k_u, & \mathrm{u>u_m} \end{cases}, \quad \omega_b(u) = \begin{cases} 0, & \mathrm{u<u_m} \\ \omega_b, & \mathrm{u>u_m} \end{cases}, \quad Q_m(u) = \begin{cases} 0, & \mathrm{u<u_m} \\ Q_m, & \mathrm{u>u_m} \end{cases}, \quad C(u) = \begin{cases} C_f, & \mathrm{u<u_m} \\ C_u, & \mathrm{u>u_m} \end{cases}.$$

The upper letter C indicates that it is the value of density multiplying specific heat in each case. Typically, $C_b = \rho_b c_b$, $C_u = \rho_u c_u$ and $C_f = \rho_f c_f$ respectively.

After implementing the heat capacity method [29], the uniform energy equation (48) can be rewritten as:

$$\tilde{C}(u) \frac{\partial u_u(\mathbf{x},t)}{\partial t} = \tilde{k}(u)\nabla^2 u_u(\mathbf{x},t) + \tilde{\omega}_b(u) C_b \left(u_a - u_u(\mathbf{x},t)\right) + \tilde{Q}_m(\mathrm{u}) \tag{49}$$

where:

$$\tilde{C}(u)=\begin{cases} C_f, & u<u_{ml} \\ \dfrac{Q_1}{u_{mu}-u_{ml}}+\dfrac{C_f+C_u}{2}, & u_{ml}\le u\le u_{ml} \\ C_u, & u>u_{mu} \end{cases}, \quad \tilde{k}(u)=\begin{cases} k_f, & u<u_{ml} \\ \dfrac{k_f+k_u}{2}, & u_{ml}\le u\le u_{mu} \\ k_u, & u>u_{mu} \end{cases},$$

$$\tilde{\omega}_b(u)=\begin{cases} 0, & u<u_{ml} \\ 0, & u_{ml}\le u\le u_{mu} \\ \omega_b, & u>u_{mu} \end{cases}, \qquad \tilde{Q}_m(u)=\begin{cases} 0, & u<u_{ml} \\ 0, & u_{ml}\le u\le u_{mu} \\ Q_m, & u>u_{mu} \end{cases}.$$

Thus, the highly non-linear problem is transformed into a linear problem at a given domain.

Figure 8 represents the whole sketch of the two-dimensional freezing problem around a cryoprobe and Figure 9 illustrates the domain and the related collocation points used for cryosurgery problem. The entire skin tissue has a length of 0.1 m in the Y direction and a width of 0.05 m along X direction.

Accounts for the complicated boundary in the cryosurgery problem, different nodes are selected for different boundaries. 20 nodes are chosen for the boundary Ⅱ ,Ⅲ and Ⅳ. A total of 110 nodes are selected over the boundary I, of which 80 nodes reside into the frozen area of cryoprobe. Moreover, there are 441 interpolation nodes in the domain of this problem. In following calculations, θ is taken to be 0.6.

Table 2 Values of properties used in freezing problem

Symbols	Value	Symbols	Value
C_b, C_u	3.6 MJ/m$^3\cdot$℃	u_a, u_c	37 ℃
C_f	1.86 MJ/m$^3\cdot$℃	u_{ml}	−8 ℃
k_f	2 W/m$\cdot$℃	u_{mu}	−1 ℃
k_u	0.5 W/m$\cdot$℃	h_∞	10 W/m$^2\cdot$℃
ω_b	0.0005 ml/s/ml	u_∞	10 ℃
Q_1	250 MJ/m^3	u_0	37 ℃
Q_m	4200 W/m^3	u_w	−120 ℃

The boundary conditions of this problem are summarized as

$$\begin{cases} k\dfrac{\partial u}{\partial x}\Big|_{x=0}=h_\infty(u-u_\infty), & \text{no contact with cryoprobe} \\ u\big|_{x=0}=u_w, & \text{contact with cryoprobe} \end{cases},$$

$$u\big|_{x=0.05}=u_c,\ q=-k\frac{\partial u}{\partial y}\Big|_{y=0}=0 \text{ and } q=-k\frac{\partial u}{\partial y}\Big|_{y=0.01}=0$$

The initial condition is simplified as $u(x,y;t)\big|_{t=0}=u_0$. The parameters used in the cryosurgery problem are listed in Table 2.

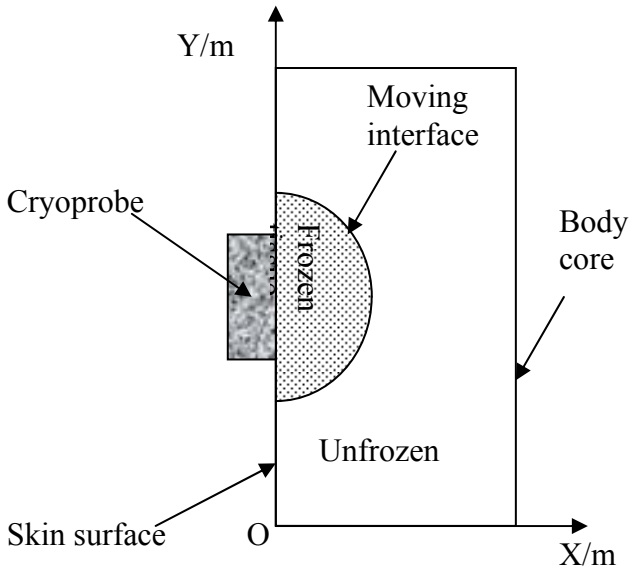

Fig. 8 Diagram of two-dimensional cryosurgery problem using one cryoprobe

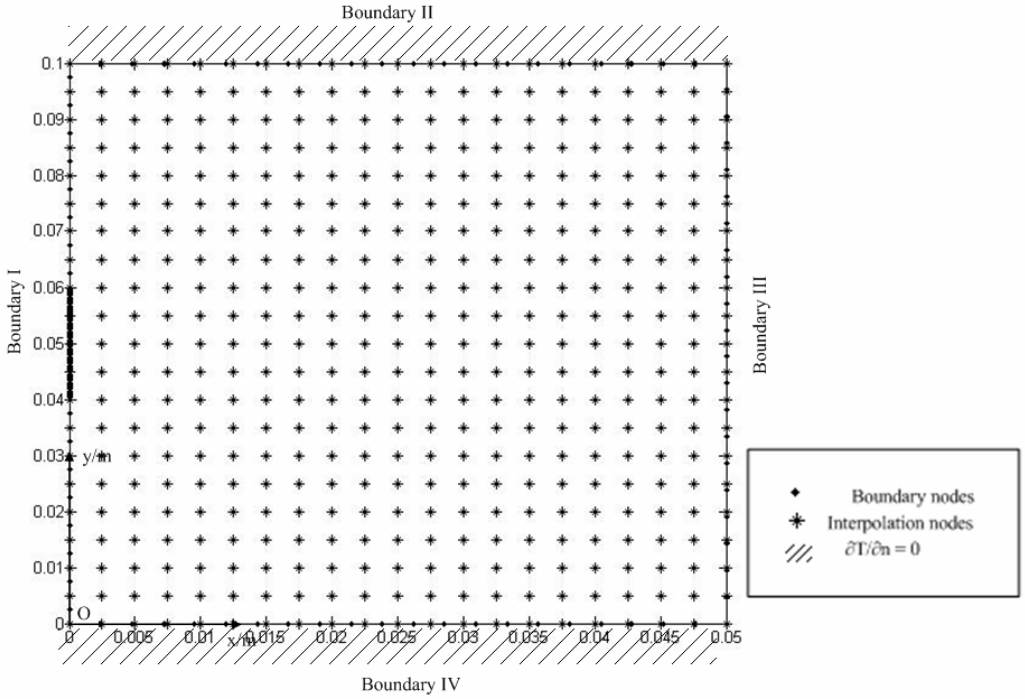

Fig. 9 Domain and nodes selection for typical cryosurgery problem

For this problem, only one cryoprobe is used to generate the freezing temperature whose size is 0.02m located at the middle of the boundary on the skin surface. Furthermore, three different time steps are considered in this analysis: Δt =10s, 100s and 1000s. The temperature distribution obtained from the proposed method is shown in Figure 10a. A more detailed and lucid isotherm map for cryosurgery problem is given by Figure 10b where the dash line and bold text indicate the lower and upper boundaries of phase change. Figure 11 represents that the upper and lower boundaries extending from the skin surface to the internal core with time changing for the case of $\Delta t = 100$. The temperature distributions versus time at the point (0.0429, 0.0543) are represented in Figure 12. They all converge to one value when the time reaches or is great than 6000s.

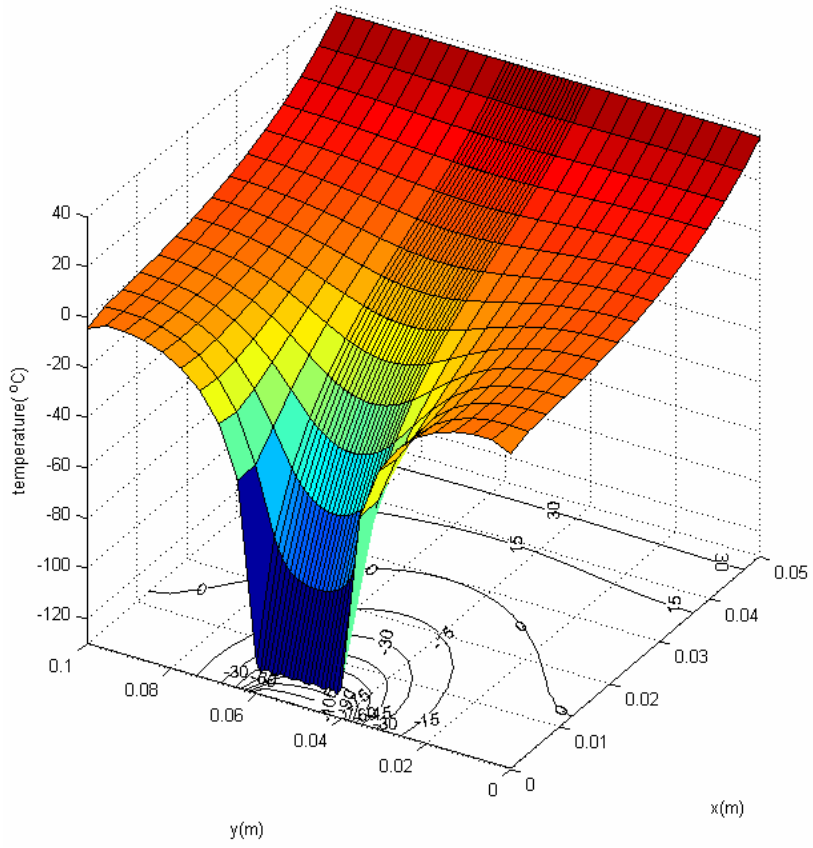

(a) Three dimensional surface graph

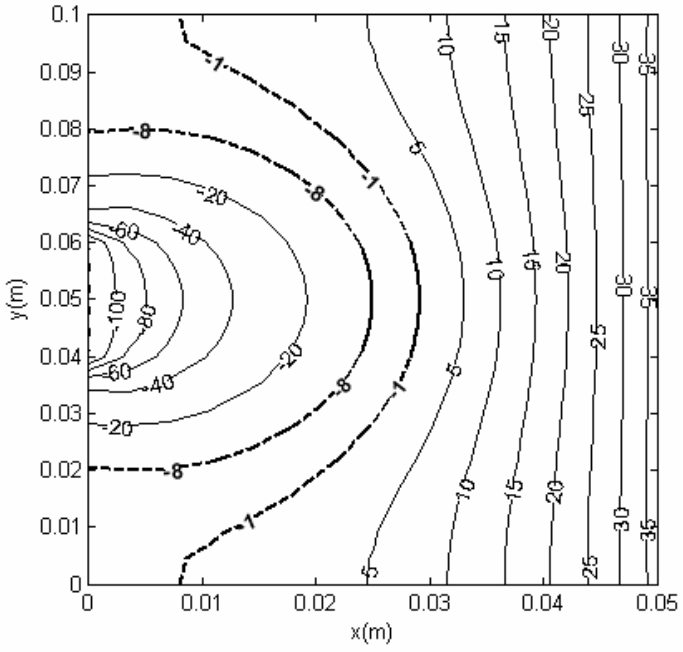

(b) Isotherm map

Fig. 10 Profile of temperature distribution at t = 1000s when Δt = 100.

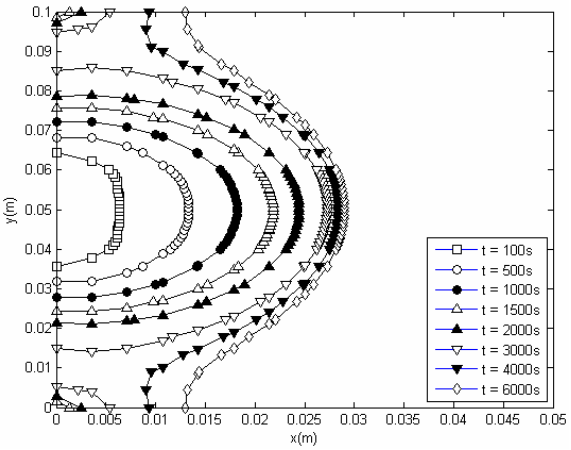

(a) Upper boundary of phase change

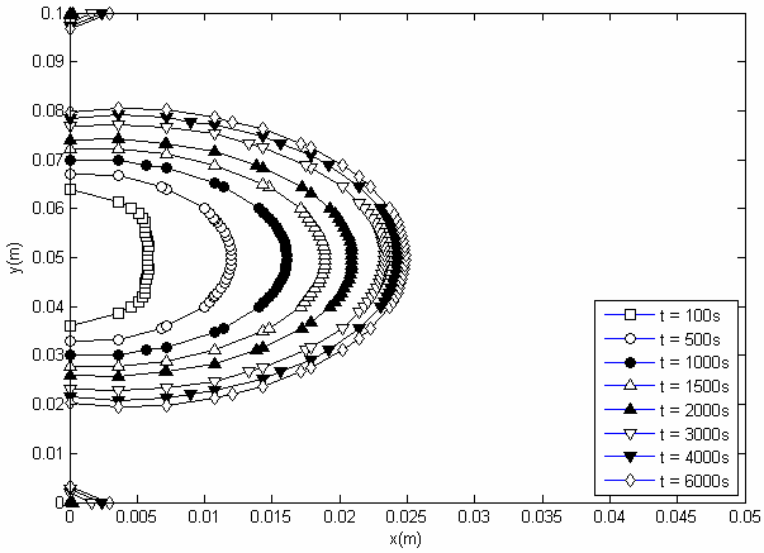

(b) Lower boundary of phase change

Fig. 11 The schematic of moving boundary of phase change versus time

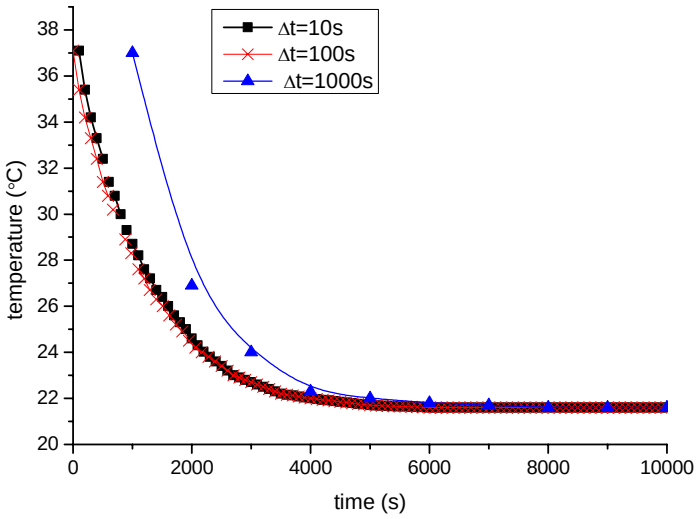

Fig. 12 Variation of temperature with time at point (0.0429, 0.0543)

4. Conclusion

From the two examples discussed above, it can be revealed that the geometry and the properties of biological tissues induce the biological heat transfer significantly complex. Analysis on the heat transfer of biological bodies consists of determination of system parameters, such as thermal conductivity, blood perfusion, specific heat or metabolic generation. This can be done by using invasive or noninvasive experiments. Another is the determination to direct problems with known parameters like temperature prediction for spatial heating. This is what we have done in the example of skin with tumor. The most complex one is the determination of non-linear problems with complicated boundary such as moving boundary and phase change.

The algorithm proposed in the paper is capable of solving these complex problems. It is shown that the computing time and accuracy of the proposed algorithm depends not only on the stepping time but also on the value of theta. Therefore, the stepping time can be selected larger as well as theta so that it can provide a faster solution process but less accurate to general biological skin problems. In practice, the stepping time is suggested to select from 50s to 200s and theta is from 0.6 to 0.9. In addition, the method can deal with various problems occurring in the skin tissues and provide a generalized numerical approach to simulate the temperature distribution and the heat flux as well.

References

1. *Qin Q.H., Ye J.Q.,* 'Thermoelectroelastic solutions for internal bone remodeling under axial and transverse loads′, *International Journal of Solids and Structures*, ***41*** *(2004), 2447-2460.*
2. *Qin Q.H., Qu C., Ye J.Q.,* 'Thermoelectroelastic solutions for surface bone remodeling under axial and transverse loads′, *Biomaterials*, ***26*** *(2005), 6798-6810.*
3. *Cao L., Qin Q.H., Zhao N.*, 'An RBF–MFS model for analysing thermal behaviour of skin tissues′, *International Journal of Heat and Mass Transfer*, ***53*** *(2010), 1298-1307.*
4. *Zhang Z.W., Wang H., Qin Q.H.,* 'Transient bioheat simulation of the laser-tissue interaction in human skin using hybrid finite element formulation′, *MCB: Molecular & Cellular Biomechanics*, ***9*** *(2012), 31-54.*
5. *Wang H.,* Qin Q.H., 'A fundamental solution-based finite element model for analyzing multi-layer skin burn injury′, *Journal of Mechanics in Medicine and Biology*, ***12*** *(2012), 125 - 127.*
6. *Tao J., Qin Q.H., Cao L.,* 'A combination of Laplace transform and meshless method for Analysing Thermal Behaviour of Skin Tissues′, *Universal Journal of Mechanical Engineering*, ***1*** *(2013), 32-42.*
7. *Pennes H.H.,* 'Analysis of Tissue and Arterial Blood Temperatures in the Resting Human Forearm′, *J. Appl. Physiol.*, ***1*** *(1948), 93-122.*
8. *Meaney P.M., Clarke R.L., Ter Haar G.R., Rivens I.H.,* 'A 3-D finite-element model for computation of temperature profiles and regions of thermal damage during focused ultrasound surgery exposures′, *Ultrasound in Medicine and Biology*, ***24*** *(1998), 1489-1499.*
9. *Torvi D.A. Dale J.D.,* 'A finite-element model of skin subjected to a flash fire′, *Journal of Biomechanical Engineering-Transactions of the Asme*, ***116*** *(1994), 250-255.*
10. *Peery J.T., Klute G.K., Blevins J.J., Ledoux W.R.,* 'A three-dimensional finite element model of the transibial residual limb and prosthetic socket to predict skin temperatures′, *Ieee Transactions on Neural Systems and Rehabilitation Engineering*, ***14*** *(2006), 336-343.*
11. *Zhao G., Zhang H.-F., Guo X.-J., Luo D.-W., Gao D.-Y.,* 'Effect of blood flow and metabolism on multidimensional heat transfer during cryosurgery′, *Medical Engineering & Physics*, ***29*** *(2007), 205-215.*
12. *Zhao J.J., Zhang J., Kang N., Yang F.Q.,* 'A two level finite difference scheme for one dimensional Pennes' bioheat equation′, *Applied Mathematics and Computation*, ***171*** *(2005), 320-331.*
13. *Rossi M.R., Tanaka D., Shimada K., Rabin Y.,* 'An efficient numerical technique for bioheat simulations and its application to computerized cryosurgery planning′, *Computer Methods and Programs in Biomedicine*, ***85*** *(2007), 41-50.*
14. *Deng Z.S., Liu J.,* 'Monte Carlo method to solve multidimensional bioheat transfer problem′, *Numerical Heat Transfer Part B-Fundamentals*, ***42*** *(2002), 543-567.*
15. Chan C.K., 'Boundary element method analysis for the bioheat transfer equation′, *Journal of Biomechanical Engineering-Transactions of the Asme*, ***114*** *(1992), 358-365.*
16. Ooi E.H., Ang W.T., Ng E.Y.K., 'Bioheat transfer in the human eye: A boundary element approach′, *Engineering Analysis with Boundary Elements*, ***31*** *(2007), 494-500.*
17. *Qin Q.H.,* 'Nonlinear analysis of Reissner plates on an elastic foundation by the BEM′, *International Journal of Solids and Structures*, ***30*** *(1993), 3101-3111.*

18. Wang H., Qin Q.H., Kang Y., 'A meshless model for transient heat conduction in functionally graded materials′, *Computational Mechanics*, ***38*** *(2006), 51-60.*

19. Wang H., Qin Q.H., 'A meshless method for generalized linear or nonlinear Poisson-type problems′, *Engineering Analysis with Boundary Elements*, ***30*** *(2006), 515-521.*

20. Wang H.,Qin Q.H., 'Meshless approach for thermo-mechanical analysis of functionally graded materials′, *Engineering Analysis with Boundary Elements*, ***32*** *(2008), 704-712.*

21. Wang H., Qin Q.H., Kang Y., 'A new meshless method for steady-state heat conduction problems in anisotropic and inhomogeneous media′, *Archive of Applied Mechanics*, ***74*** *(2005), 563-579.*

22. Gowrishankar T.R.,Stewart D.A., Martin G.T., Weaver J.C., 'Transport lattice models of heat transport in skin with spatially heterogeneous, temperature-dependent perfusion′, *Biomedical Engineering Online*, ***3*** *(2004), 42.*

23. Qin Q.H., Wang H., 'Matlab and C programming for Trefftz finite element methods', CRC Press, Taylor & Francis, Boca Raton, *2008.*

24. Wang H., Qin Q.H., 'Fundamental-solution-based finite element model for plane orthotropic elastic bodies′, *European Journal of Mechanics-A/Solids*, ***29*** *(2010), 801-809.*

25. Smith I.M., Griffiths D.V., 'Programming the finite element method (4th edition)', John Wiley & Sons, Ltd, Hoboken *2004.*

26. Liu J., Xu L.X., 'Boundary information based diagnostics on the thermal states of biological bodies′, *International Journal of Heat and Mass Transfer*, ***43*** *(2000), 2827-2839.*

27. Lv Y.G., Deng Z.S., Liu J., '3-D numerical study on the induced heating effects of embedded micro/nanoparticles on human body subject to external medical electromagnetic field′, *Ieee Transactions on Nanobioscience*, ***4*** *(2005), 284-294.*

28. DudarT.E.,Jain R.K., 'Differential response of normal and tumor microcirculation to hyperthermia′, *Cancer Research*, ***44*** *(1984), 605-612.*

29. Deng Z.S., Liu J., 'Modeling of multidimensional freezing problem during cryosurgery by the dual reciprocity boundary element method′, *Engineering Analysis with Boundary Elements*, ***28*** *(2004), 97-108.*